JOURNAL OF PROPULSION AND POWER
Vol. 16, No. 6, November–December 2000

# Regenerative Solid Oxide Fuel Cells for Mars Exploration

K. R. Sridhar*
*University of Arizona, Tucson, Arizona 85719*
and
R. Foerstner†
*Universität Stuttgart, D-7550 Stuttgart, Germany*

**A regenerative solid oxide fuel cell was designed, built, and tested for Mars exploration. The fuel cell operates at night on CO and excess $O_2$ generated during the day from the Mars atmospheric $CO_2$. The primary objective of the device was to generate $O_2$ from the Mars atmosphere for use as an ascent vehicle propellant. The cells tested were composed of an 8-mol% yttria-stabilized zirconia electrolyte and two platinum electrodes. The results obtained from the experimental tests were consistent with the theoretical relations predicted by thermodynamics and electrochemistry. The performance loss of the fuel cell, observed during the first 40 h of operation in the fuel cell mode, was attributed to chemisorption of CO by the platinum electrodes. It was found that the concentration overpotential was negligible and the calculated activation overpotential fit well with the Tafel equation. The results suggest that operating $O_2$ generator cells as fuel cells with low fuel utilization at night has advantages for Mars missions.**

## Introduction

REGENERATIVE fuel cells (RFCs) have been considered as potential energy-storage devices for several space missions, including lunar bases[1] and human missions to Mars.[1,2] The concept relies on an electrochemical device that can be reversed periodically to convert electrical energy to chemical energy and vice versa. The electrochemical device in this case is a stack of cells that performs as an *electrolyzer*, or a *fuel cell*. In the fuel-cell mode, the stack of cells converts chemical energy via an electrochemical reaction that utilizes a fuel and oxidant to form a reaction product. In the electrolyzer mode, the reaction product is converted and separated to fuel and oxidant by utilizing electrical energy. Elegant schemes for energy storage have been suggested using this concept,[1,2] and they are very attractive when the primary source of energy for a mission is solar. On a lunar base, for example, the RFC would operate as an electrolyzer to produce fuel and oxidant during most of the lunar day (about 336 h) using power from solar photovoltaic arrays. For the lunar night (about 336 h), the RFC would utilize the fuel and oxidant to produce the required electric power.

One of the primary distinctions between the RFCs and other energy storage devices, such as batteries, is that the total energy needed and the power required are not as closely coupled for RFCs as they are for batteries. If the same amount of power is required for a longer period of time (i.e., more energy), then the sizes of the fuel and oxidant tanks have to be increased, but not the size of the cell stack. Therefore, for applications where power is needed for long periods, the mass advantage offered by a RFC is significant in comparison to traditional primary or secondary batteries. Past papers have focused on using solid-polymer electrolyte-based fuel cells with Earth-carried hydrogen and $O_2$ (or water) as the reactants.[1,2]

This paper focuses on a solid-oxide electrolyte-based fuel cell that will use CO and $O_2$ as reactants. The reactants are obtained by electrolyzing the $CO_2$ in the atmosphere of Mars. There are two important distinctions between the solid polymer- and the solid oxide-based RFC concepts: 1) All of the fluids in the solid-oxide system are gaseous, as opposed to the liquid–vapor mixture encountered in the solid polymer. 2) The working fluid for the RFC is obtained from Mars for the solid oxide system, as opposed to being carried from the Earth for the solid polymer system. Unlike the RFCs considered in the past, the primary application of the device presented in this paper is not energy storage. The cell stack will primarily produce $O_2$ for the return vehicle's propulsion needs. The advantage of producing $O_2$ by electrolyzing the predominantly $CO_2$ atmosphere of Mars for return vehicle propulsion has been discussed in detail elsewhere.[3,4] The excess capacity of the cell stack will be utilized to produce small amounts of excess $O_2$. This excess $O_2$ will be combined with the CO that is produced as a product of the electrolysis reaction and will be used to operate the stack as a fuel cell during the night. This stack will produce limited amounts of electrical power for the nighttime needs of the rest of the spacecraft. Because the fuel cell reaction is exothermic, it will keep the electrolyzer stack warm during the night and thereby eliminate the need to thermally cycle the stack diurnally if the mission relies solely on solar power. If thermal cycling on a diurnal basis is eliminated, the reliability of the device is greatly enhanced. By maintaining the stack at operating temperature day and night, the time needed for thermal ramp-up each Martian day (after the solar cells start generating sufficient power) is eliminated, thereby increasing the total available time for $O_2$ production time. In addition, when operating in the fuel-cell mode, the RFCs will provide high- and moderate- temperature heat to the rest of the spacecraft during the cold Martian night.

Experiments were conducted in the laboratory to characterize the solid oxide cell in the RFC mode and prove the feasibility of the concept. A brief explanation of the principle of operation of the solid oxide cell is followed by a description of the experimental setup. The results of the experiments are reported, and the significance of the results is discussed.

## Principle of Operation

The solid-oxide electrolyte is an $O_2$ ion conductor. The electrolyte considered is 8-mol% yttria-stabilized zirconia (YSZ). Oxygen ion vacancies in the crystal structure of the electrolyte permit the transport of $O_2$ from the cathode to the anode when an electric potential is applied. Alternatively, a large $O_2$ partial-pressure difference across the electrolyte, and the presence of a fuel on the low $O_2$ concentration side, will allow for an electrochemical reaction to occur as a result of $O_2$ ion transport across the electrolyte and electron flow in the external circuit (power generation).

For both electrolyzer and fuel cell reaction to occur, electrons must be transported to or from the reaction site. This is done by

Presented as Paper 98-0650 at the AIAA 36th Aerospace Sciences Meeting, Reno, NV, 12–15 January 1998; received 12 March 1999; revision received 1 October 1999; accepted for publication 20 October 1999. 

*Associate Professor, P.O. Box 210119, Department of Aerospace and Mechanical Engineering. Associate Fellow AIAA.

†Ph.D. Candidate, Institut für Raumfahrtsysteme, Pfaffenwaldring 31.

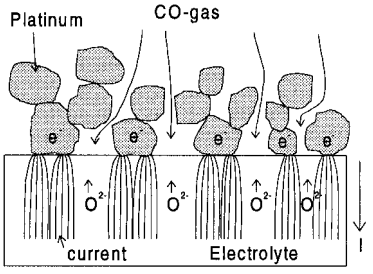


**Fig. 1 Three-phase boundary at the electrode–electrolyte interface.**

means of porous electrodes that are directly attached to the surface of the electrolyte. For the electrochemical reaction to occur, the fuel molecules and the $O_2$ ions must make contact, and the electrons must be transported to or from the site. This condition exists only where the fuel, the electrode, and the electrolyte meet. This is the so-called three-phase boundary (Fig. 1), which is the only place where the electrochemical reaction can take place.

### Cell Reactions

The fuel cell half-cell reactions for the CO and $O_2$ reactants are, for the anode,

$$CO + O^{2-} \rightarrow CO_2 + 2e^- \tag{1}$$

and $\Delta h^0_{298,a} = -532{,}180$ J/mol (Ref. 5). For the cathode,

$$\tfrac{1}{2}O_2 + 2e^- \rightarrow O^{2-} \tag{2}$$

and $\Delta h^0_{298,c} = 249{,}190$ J/mol (Ref. 5).

The overall cell reaction is

$$CO + \tfrac{1}{2}O_2 \rightarrow CO_2 \tag{3}$$

where

$$\Delta h^0_{298,\text{cell}} = -282{,}990\ \text{J/mol}_{CO_2}$$

where the superscript 0 stands for standard pressure (partial pressure, 1.013 bar); the subscript gives the temperature; $a$ and $c$ stand for anode and cathode, respectively; and $e^-$ stands for an electron. A negative enthalpy value denotes an exothermic reaction. The subscript $CO_2$ in Eq. (3) indicates the energy released when one mole of $CO_2$ is formed. For an ideal cell, the amount of this enthalpy that is available as electrical energy is given by the Gibbs free energy equation,

$$w_{\text{el}} = \Delta g = \Delta h_r - T \cdot \Delta s \tag{4}$$

where $w_{\text{el}}$ is the specific electrical work provided by an ideal cell, $\Delta h_r$ is the specific enthalpy of reaction, $\Delta g$ is the change in specific Gibbs free energy, $T$ is the reaction temperature, and $\Delta s$ is the change in specific entropy.

### Reversible Cell Voltage

The relation between the Gibbs free energy and reversible cell voltage $E_r$ is given by

$$E_r = -\Delta g/(n \cdot F) \tag{5}$$

where $F$ is the Faraday constant, 96,493 C/mol and $n$ is the number of electrons transported for each molecule that is reacted.

For reaction (3) the Nernst reaction is given by

$$E_r = (\Re \cdot T)/(n \cdot F) \cdot \ln(K) + (\Re \cdot T)/(2 \cdot n \cdot F) \cdot \ln\left(p_{O_{2,c}}\right) + (\Re \cdot T)/(n \cdot F) \cdot \ln\left(p_{CO}/p_{CO_2}\right) \tag{6}$$

This is the Nernst equation for the tested fuel cell. The equilibrium constant $K$ for different temperatures can be calculated using following approximation:

$$K = (1/c_d) \cdot e^{[E_d/(\Re \cdot T)]} \tag{7}$$

For reaction (3), $c_d = 3.5 \times 10^4$ and $E_d = 282.8$ kJ/mol (Ref. 6).

Equation (6) can be used to calculate the dependence of the reversible cell potential on pressure, temperature, and fuel utilization. The dependence relationships for reaction (3) are presented in Eqs. (8), (9), and (10), respectively:

$$E_r(T)|_{p,\mu} = E_d/(n \cdot F) - (\Re \cdot T)/(n \cdot F) \cdot \ln(c_d) + (\Re \cdot T)/(2 \cdot n \cdot F)\ln\left(p_{O_{2,c}}\right) + (\Re \cdot T)/(n \cdot F) \cdot \ln\left(p_{CO}/p_{CO_2}\right) \tag{8}$$

$$E_r(p)|_{T_1,\mu_1} = E_r(T_1, \mu_1) - \frac{\Delta v \cdot \Re \cdot T}{n \cdot F} \cdot \ln\left(\frac{p}{p_1}\right) \tag{9}$$

$$E_r(\mu)|_{T,p} = (\Re \cdot T)/(n \cdot F) \cdot \ln(K) + (\Re \cdot T)/(2 \cdot n \cdot F)\ln\left(p_{O_{2,c}}\right) + (\Re \cdot T)/(n \cdot F) \cdot \ln[(1-\mu)/\mu] \tag{10}$$

where $\Delta v$ is the stoichiometric constant, and the fuel utilization $\mu$ is defined by

$$\mu = \frac{p^{\text{in}}_{CO} - p^{\text{out}}_{CO}}{p^{\text{in}}_{CO}} \tag{11}$$

### Cell Irreversibilities

The reversible cell potential as shown in Eq. (10) applies to a cell only when it is in equilibrium, that is, no current is flowing through the cell or no species is transported. Potential barriers are created due to both charge concentrations at the electrode/electrolyte interface and concentration gradients between the bulk flow and at the three-phase boundary. The increases in cell potentials due to these two factors are called activation and concentration overpotentials, respectively. The relationship between current density and activation overpotential for a cell is given by the Butler–Volmer equation,

$$i = i_0 \cdot \left\{ \exp\left[\frac{(1-\alpha)\eta_{ac} \cdot n \cdot F}{\Re \cdot T}\right] - \exp\left[\frac{\alpha \cdot \eta_{ac} \cdot n \cdot F}{\Re \cdot T}\right] \right\} \tag{12}$$

where $i$ is the current density, $i_0$ is the exchange current density (a constant for a given cell operating at a fixed temperature and pressure), $\alpha$ is the transport coefficient (a constant between 0 and 1), and $\eta_{ac}$ is the activation overpotential.

Equation (12) can be simplified for high positive activation overpotentials. In this case, the second term in Eq. (12) can be neglected. The simplified equation can be solved for $\eta_{ac}$ to obtain the Tafel equation,

$$\eta_{ac} = -\frac{\Re \cdot T}{(1-\alpha) \cdot n \cdot F} \cdot \ln i_0 + \frac{\Re \cdot T}{(1-\alpha) \cdot n \cdot F} \ln i = a + b \cdot \ln i \tag{13}$$

Because $O_2$ ions are transported across the electrolyte and chemical reactions occur at the electrodes, there is a concentration gradient between the bulk flow in the cell and at the electrode/electrolyte interface. This concentration barrier increases the cell potential in an electrolyzer and decreases it in a fuel cell. Obviously, the maximum cell current will occur when the concentration of the $O_2$ ions at the electrode is zero. The cell current for this condition is called the limiting current. Using Ficks law of diffusion and charge balance, the limiting current density $i_L$ can be shown to be

$$i_L = n \cdot F \cdot D \cdot (c_{\text{ion}}/\delta) \tag{14}$$

where $D$ is the diffusion coefficient, $\delta$ is the thickness of the diffusion layer according to the Nernst approximation, and $c_{\text{ion}}$ is the concentration of the ions outside the diffusion layer in the bulk.

From analysis, it can be shown that the concentration overpotential can be expressed as

$$\eta_D = (\Re \cdot T)/(n \cdot F) \cdot \ln[1 - (i/i_L)] \tag{15}$$

and the cell current can be expressed as

$$i = i_L \cdot \left\{1 - \exp\left[\frac{n \cdot F \cdot \eta_D}{\Re \cdot T}\right]\right\} \tag{16}$$

Ohmic resistance accompanies the transfer of electrical charge. It occurs due to the ionic resistance in the electrolyte, electronic resistance in the electrodes, and contact resistance. It can be expressed by the equation

$$\eta_\Omega = I \cdot R_\Omega \tag{17}$$

where $R_\Omega$ is the total cell resistance from all sources.

The potential-current relation is the most important relation in specifying the performance of a cell. The relation is given by

$$U(I) = E_r - |\eta_{ac}| - |\eta_D| - \eta_\Omega = E_r - |(\Re \cdot T)/(\beta \cdot n \cdot F)\, \ln(I/I_0)| - |(\Re \cdot T)/(n \cdot F)\, \ln[1 - (I/I_L)]| - I \cdot R_\Omega \tag{18}$$

## Experimental Setup

### Cell Configuration

The test cell consisted of a cold-pressed and sintered nonporous 8-mol% YSZ electrolyte disk that was sandwiched between two YSZ crucibles (Coors Ceramic Company). The diameter of the disk was 28 mm. The thickness of the electrolyte disks ranged from 600 to 750 $\mu$m. Platinum was chosen as the electrode material, and it was painted in paste form on the YSZ disk and fired. The reasons for selecting platinum as the electrode material were its high catalytic activity, its chemical stability both at high temperatures and in oxidizing environments, its ease of handling, and the ease of procuring the material in pure form. In the future, other electrode materials will be considered that are conductive to both electrons and oxygen ions, so-called mixed conductors, for example, $La_{0.7}Sr_{0.3}Mn_{3-x}$ (Ref. 7). The electrode area was approximately 2 cm.$^2$ The crucibles were sealed to the electrolyte disk using a ceramic cement (Aremco Products, Inc.) that was painted in paste form on the YSZ disk and fired. The electrodes were connected to the terminals of the testbed via platinum wires (Alfa Aesar). The connection between the platinum wire and the electrodes was made by forming a spiral, flattening it, and attaching it to the electrodes with platinum paste. A detailed description of the entire building process is given by Sridhar and Vaniman.[8] A schematic of the cell configuration can be found in Fig. 2.

### Testbed

A schematic of the testbed is shown in Fig. 3. The cell was situated inside a custom-fabricated ceramic fiber heater (Watlow) that was

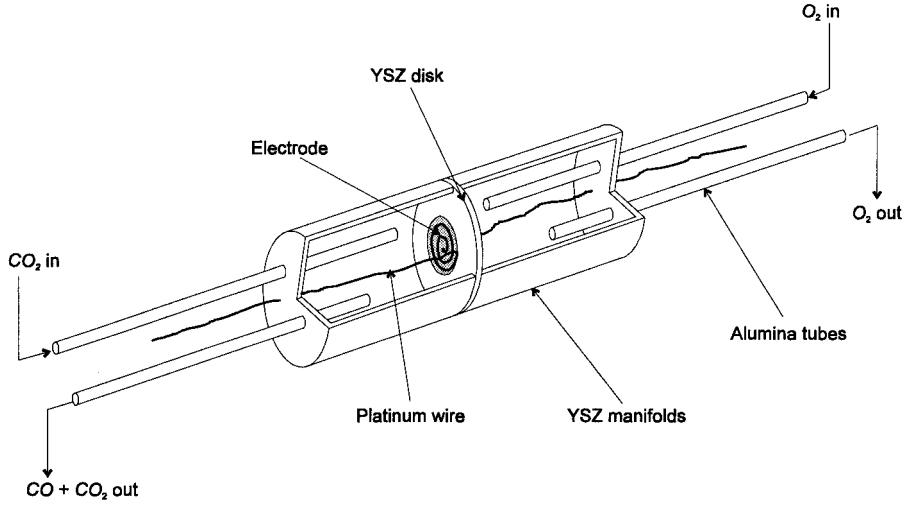


**Fig. 2 Cutaway of the cell configuration.**

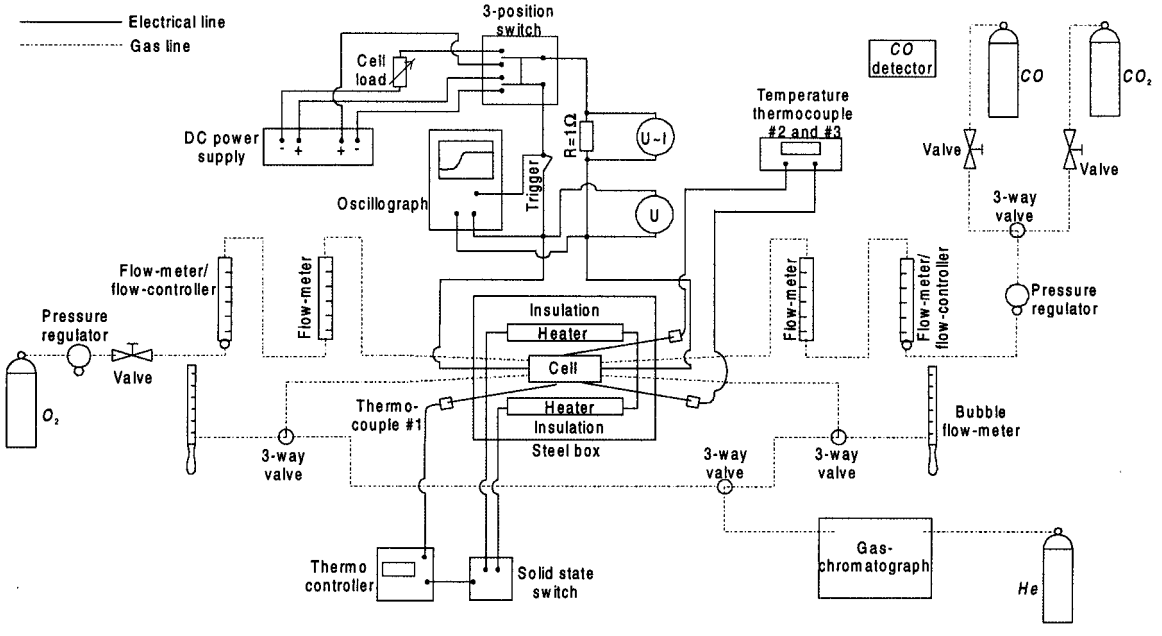


**Fig. 3 Schematic of testbed.**

placed in a steel box. The box was filled with ceramic blanket insulation (Koawool®, Thermal Ceramics). The heater was controlled by a Watlow thermal controller (Series 942) via a solid state relay. The temperature in the testbed was measured by three shielded, ungrounded type K thermocouples (Omega). The thermocouples were placed at different locations within the testbed. The load for the fuel cell was an adjustable resistor (5–1000 Ω). By means of the three-position switch, the cell circuit could be interrupted, switched to the cell load for fuel cell mode (FCM), or connected to the power supply so that it would operate in the electrolyzer mode (ELM). Note that the $O_2$ side is called cathode in the FCM and anode in the ELM. The opposite is true for the fuel side. An oscilloscope measured the cell voltage at the same place as the voltmeter. For measuring the ohmic overpotential using the current interrupt method, it was necessary to break the cell circuit and trigger the oscilloscope. The cell was supplied with gas by three high-pressure gas cylinders. The purity of the $O_2$ and $CO_2$ gases was 99%; the purity of the CO was 98%. The pressure of the gases was downregulated to 5 psig before they were fed to the cell. A Shimadzu GC-8A gas chromatograph was used to determine the composition of the gases coming out of the cell. The exhaust gas lines were set up in such a way that the gases from both sides could be sent either to a bubble flow meter or to the gas chromatograph.

## Results and Discussion

### Electrolyzer Characteristics

The performance of the electrochemical cell in the electrolyzer mode is shown in Fig. 4. The performance of the cell increased with increasing temperature, corroborating previous results.[8] Also, the performance of the cell remained fairly constant over prolonged periods of operation in the electrolyzer mode.

### Fuel Cell Characteristics

The performance of the cell in the FCM at 850°C is shown in Fig. 5. The shape of the current–voltage relationship is qualitatively consistent with theoretical predictions presented in Eq. (18) at low and intermediate current levels. At low current levels, the voltage drop was primarily due to activation overpotential and, at the intermediate current levels (the linear portion of the curve), the potential drop was dominated by the ohmic losses. At the highest current levels, the curve was predicted to drop drastically, to zero potential, due to diffusion limits. The experimental curve deviated from this prediction, possibly due to the chemisorption process described hereafter and also due the mass-limiting flow conditions created at the highest current levels.

### Performance Degradation

Degradation in performance was observed when the cell was operated for prolonged periods in the FCM. Cell performances for two different cells operated at 900°C and 950°C in the FCM are shown in Figs. 6a and 6b. The degradation behavior was also exhibited at an operating temperature of 850°C.

These and other measurements of cell performance indicated two trends: 1) The degradation rate was higher at higher operating temperatures. 2) The rate of degradation at any temperature seemed to taper off with time. The degradation rate dropped significantly after 40 h of continuous operation in the FCM. This was confirmed by an endurance test where the cell was run for 310 h in the FCM. Before the endurance test, the cell was run for more than 40 h in the FCM, and, during this time, the performance dropped as shown in Figs. 6a and 6b. After the 40 h, the degradation stabilized, as can be seen in Fig. 7. The voltage-current (V-I) characteristics of the cell before the endurance test, where it was already running for 40 h in the FCM, are almost identical to the characteristics after 310 h. This result confirms that the rate of performance degradation was insignificantly small after approximately 40 h in the FCM.

Based on these observations, it was postulated that the degradation in performance was due to a reduction in the catalytic activity of platinum that resulted from the chemisorption of CO. The chemisorbed CO at the platinum surface is oriented in such a way that the carbon atom is directly combined with the platinum, and the oxygen atom is covering the carbon atom and protecting it from action with oxygen molecules that strike the surface.[9] Thus, the CO blocks reaction sites and the performance of the cell decreases.[10] The platinum surface gets rid of the CO only by evaporation of the

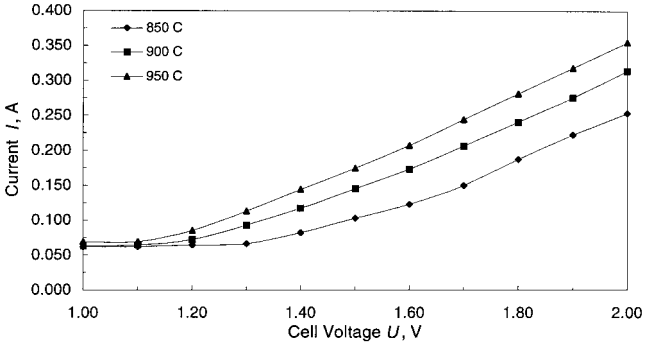


**Fig. 4 Current–voltage relation for different temperatures (ELM, $A_{el}$ = 2 cm$^2$).**

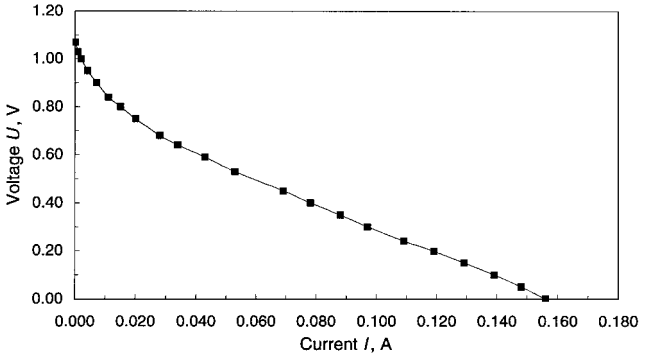


**Fig. 5 Current–voltage relationship at 850°C.**

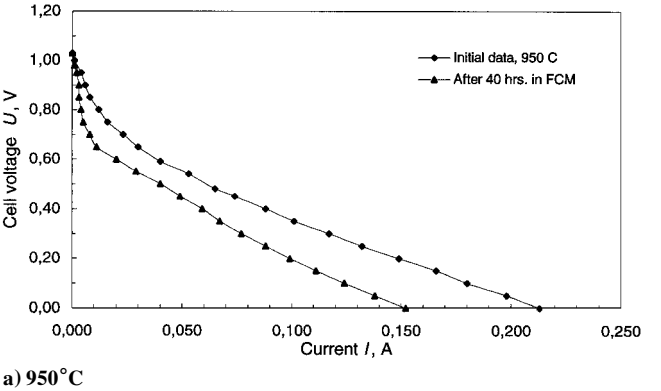


**a) 950°C**

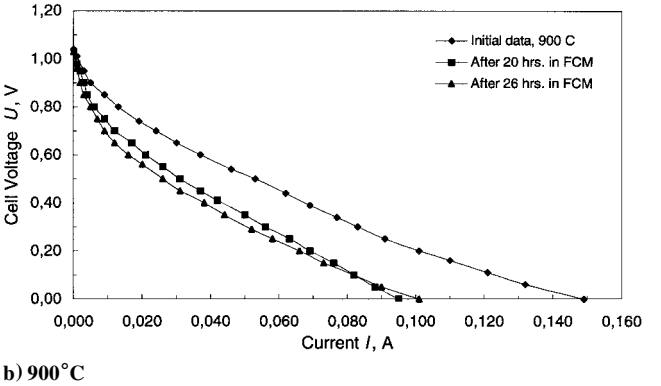


**b) 900°C**

**Fig. 6 Characteristics of the current–voltage relation over time ($A_{el}$ = 2 cm$^2$).**

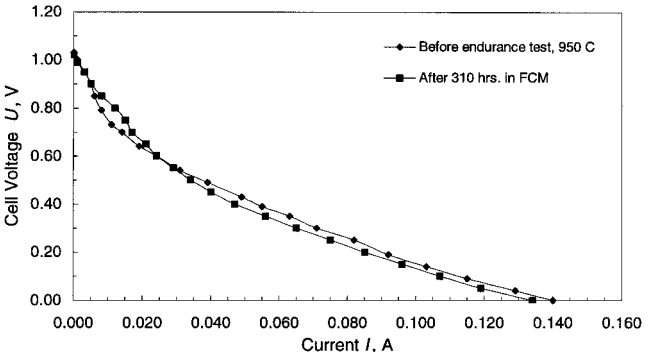


**Fig. 7 Cell performance before and after 13 days in the FCM ($A_{el}$ = 2 cm$^2$) after a previous 40 h in the FCM.**

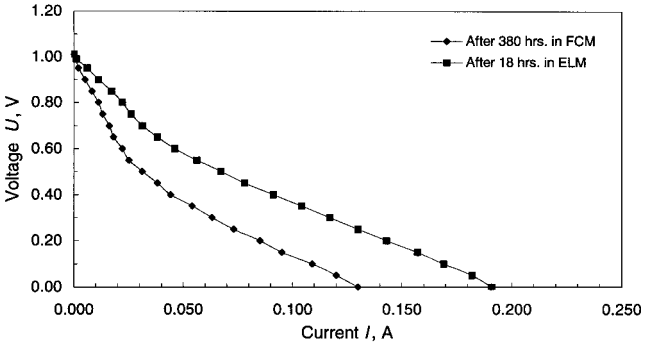


**Fig. 8 Cell performance at 950°C before and after running it in the ELM ($A_{el}$ = 2 cm$^2$).**

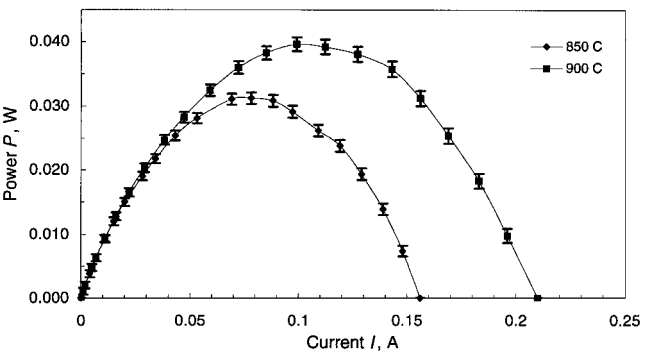


**Fig. 9 Power output of the cell as a function of current ($A_{el}$ = 2 cm$^2$).**

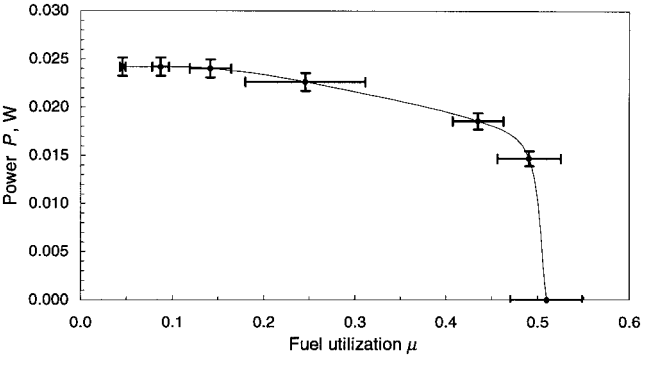


**Fig. 10 Power output $P$ vs fuel utilization $\theta$ ($T$ = 950°C).**

adsorbed CO. The rate of evaporation is increased by either raising the temperature or lowering the partial pressure of CO in the bulk gas. If this is indeed the case, it would be possible to recover cell performance, at least partially, by flowing $O_2$ through the electrodes. Two different experiments were conducted: One involved running the cell in the EM periodically to rid the platinum of the chemisorbed CO, and the other involved flushing the electrodes with $O_2$ between tests. Both techniques provided very good cell recovery. The results of operating the cell in the EM are presented in Fig. 8 for 950°C. It can be seen that, even after 380 h of continuous operation in the FCM, the cell recovered quickly when operated in the EM. Such behavior was also observed at 850 and 900°C cell operating temperatures. The fuel cell performance also recovered when it was flushed with $O_2$ gas.

These results validate the postulation of cell degradation due to chemisorption. A performance characteristic for the fuel cell is the current at a zero cell potential, the short circuit current (SCC). SCCs will vary with time of operation due to cell degradation. They varied from 0.213 A at 950°C at the beginning of life to 0.134 A after 310 h of operation.

### Transference Numbers and Open Circuit Voltage (OCV)

The Faradaic efficiency of the cell provides the ratio of the ionic conductivity across the cell to the total (electronic and ionic) conductivity. This number, ranging from 0 to 1 (also termed the transference number), is obtained by comparing the mass flow of $O_2$ to the measured current. Within the experimental error, it was found to be unity for the cells tested. The measured open circuit voltage (OCV) for the cells corresponds to the theoretical reversible cell voltage $E_r$ discussed earlier. It was found to be between 0.07 and 0.08 V for the electrolyzer and ranged from 1.03 to 1.07 V for the fuel cell.

### Power Output

The power output of the fuel cell is plotted as a function of current for operation temperatures of 850 and 900°C in Fig. 9. The maximum power output was always attained at a current value that was slightly below one-half of the SSC. The maximum peak power attained was 40 mW at 900°C at a load of about 4$\Omega$.

The power output was also measured at various $CO_2$ flow rates to compute its relationship with fuel utilization. This graph is presented in Fig. 10. For fuel utilizations higher than 45%, the power output dropped rapidly. For all other tests the fuel utilization was kept at about 9%, the portion of the curve where the power is independent of $\mu$, to remove its effect from the cell performance. The output power was found to be independent of the $O_2$ flow rate on the cathode side. The experiments showed that maintaining a pressurized cathode chamber without any through flow was sufficient on the $O_2$ side.

### Ohmic Overpotential

The ohmic cell resistance was obtained by measuring the transient characteristics of the cell voltage by means of an oscilloscope when the external circuit was interrupted. If the circuit is switched off, the cell voltage increases back to the OCV because overpotentials become zero. This method relies on the fact that the ohmic overpotential decays much more quickly than the activation and concentration overpotentials. The ohmic overpotential is the voltage drop across the ohmic resistance of the cell. This resistance is only felt if a current flows. At the moment the external circuit is opened, the current stops. Thus, the ohmic overpotential ceases to influence the measuring instrument in a time comparable with the relaxation time of the electrons in the metal, a time below $10^{-10}$ s (Ref. 11). Because this time is very small, it can be said that the cell voltage increases instantaneously by the value of the ohmic overpotential if the external circuit is opened. The activation and concentration overpotentials occur because of electrochemical reaction and diffusion, respectively. These processes do not stop as fast as the movement of the electrons. Hence, the activation and concentration overpotentials cease to influence the measurement at a much slower time scale than the ohmic overpotential. According to electrochemical literature,[12] the time before the activation and concentration overpotential start to decrease is larger than about $10^{-5}$ s for low-temperature fuel cells.

Note that although the electrolyte disk resistance decreased with increasing temperature due to increased ionic conductivity, the lead

**Table 1 Ohmic cell resistance at different temperatures**

| Temperature $T$, °C | Resistance $R_\Omega$, $\Omega$ | Error (±), $\Omega$ | Standard deviation, $\Omega$ |
|---|---|---|---|
| 850 | 2.6 | 0.3 | 0.2 |
| 900 | 2.5 | 0.3 | 0.1 |
| 950 | 2.7 | 0.4 | 0.2 |

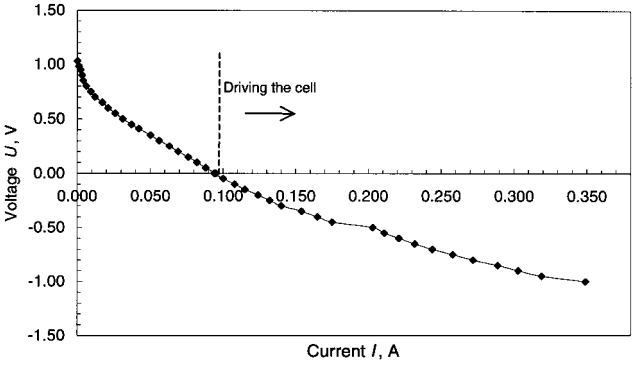


**Fig. 11 Limiting current test at 900°C ($A_{el}$ = 2 cm$^2$).**

wire and contact resistance increased with increasing temperature. Because of these counteracting contributions, no trend was observed in the measured ohmic cell resistance. The data are summarized in Table 1.

### Concentration Overpotential

The limiting current is reached when the ion concentration $c_e$ in the electrolyte at the three-phase boundary becomes zero. The influence of the concentration overpotential decreases as this current increases. Further, if the limiting current $i_L$ is known, the concentration overpotential can be calculated [see Eq. (15)]. To determine the limiting current, the voltage of the power supply that was connected to the cell was increased until the cell voltage went negative. This means the resistance the cell feels was virtually negative and the cell was driven by the power supply. If the limiting current is reached, the current should not increase any more, although the voltage is increased further. The results of this experiment at 900°C are shown in Fig. 11. The results at other temperatures showed similar trends.

It is apparent that the limiting current was not reached in the experiment. From Eq. (15), it can be shown that, for a cell current of 220 mA and a limiting current of 900 mA, the concentration overpotential was about 8.5 mV. This suggests that the concentration overpotential was negligible for the conditions that were tested.

### Activation Overpotential

Tafel plots give the relation between the activation overpotential and current. The activation overpotential was obtained by neglecting the concentration overpotential and subtracting the ohmic overpotential from the total overpotential:

$$\eta_{ac} = \underbrace{\mathrm{OCV} - U}_{\text{total overpotential}} - I \cdot R_\Omega \qquad (19)$$

Figure 12 shows an example of a Tafel plot at 900°C. The area of low activation overpotential and the area of high overpotential are not always linear. The area in between usually shows an almost linear relation between $\eta_{ac}$ and log $I$. This linear area was taken to fit a line by the method of least squares, as shown in Fig. 13. The equation obtained by matching a line is

$$\eta_{ac} = 0.7154 + 0.102 \cdot \ln(I) \qquad (20)$$

### Current–Voltage Characteristics

For the design of a RFC system, it is important to be able to make predictions of the current–voltage relation, because this is the most important characteristic of a fuel cell. In the preceding sections, the overpotentials and reversible cell voltage were evaluated. Using these results, the current–voltage relation of a cell can be predicted with Eq. (18). Figures 14a and 14b compare the actual performance of a fuel cell at 950°C with that of the prediction from Eq. (18) using the experimentally obtained constants. The results compared are in close agreement, suggesting that most of the physics are captured by the modeling.

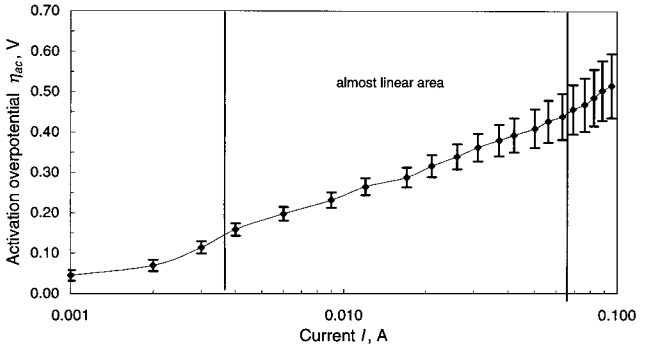


**Fig. 12 Tafel plot at 900°C ($A_{el}$ = 2 cm$^2$).**

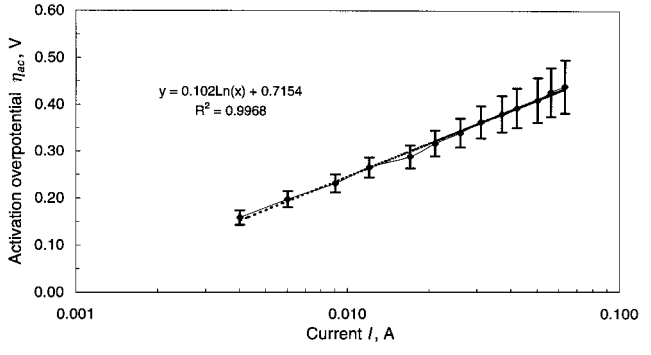


**Fig. 13 Tafel plot of linear area corresponding to Fig. 12 ($A_{el}$ = 2 cm$^2$).**

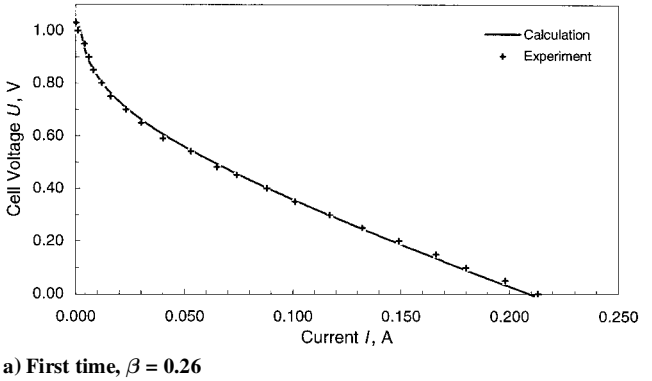


**a) First time, $\beta$ = 0.26**

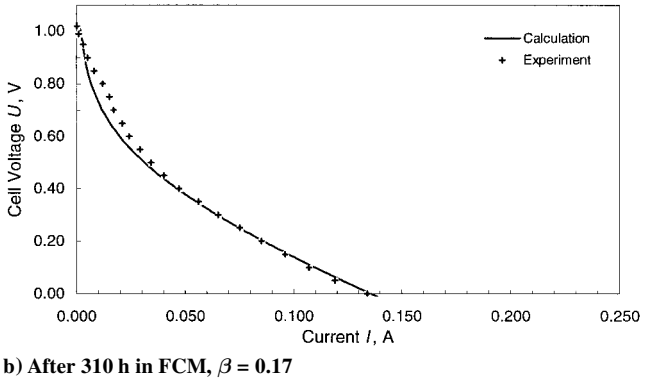


**b) After 310 h in FCM, $\beta$ = 0.17**

**Fig. 14 Comparison of experimental data for cell 2 at 950°C with the calculated prediction ($I_0$ = 1.713 mA and $R_\Omega$ = 2.6 Ω).**

## Conclusions

The results of this work show that it is possible to run a solid oxide electrolyzer cell as a regenerative fuel cell with CO as fuel and $O_2$ as oxidizer. It was found that the performance of the cell decreases in the FCM and becomes stable after approximately 40 h of operation. This is probably due to a strong chemisorption of CO by the platinum electrodes. It was further shown that a recovery of the performance is possible by running the cell for a few hours in the EM. In the future, different electrode materials that are not susceptible to degradation will be explored.

By means of measuring the transient characteristics of the cell voltage, it was possible to determine the ohmic resistance of the cell. It showed no particular dependence on the cell temperature or operation time. The limiting current of the cells could not be determined because it was higher than 800 mA. Because the limiting current was at least four times the maximum current of the tested cells, it was reasonable to neglect the concentration overpotential. By knowing the ohmic resistance and neglecting the concentration overpotential, it was possible to calculate the activation overpotential. By fitting a line to the Tafel plots, the electrochemical constants $I_0$ and $\beta$ were determined. Using these constants, it was possible to predict the performance of a solid-oxide fuel cell.

## References

[1]McElroy, J. F., Molter, T. W., and Mouthrop, L. C., "SPE Regenerative Hydrogen/ Oxygen Fuel Cells for a Lunar Base Power System," *Proceedings of the 25th Intersociety Energy Conversion Engineering Conference—IECEC '90*, American Inst. of Chemical Engineers, New York, 1990, pp. 143–148.

[2]Littman, F. D., Cataldo, R. L., McElroy, J. F., and Stedman, J. K., "Long Life Regenerative Fuel Cell Technology Development Plan," *Proceedings of the 27th Intersociety Energy Conversion Engineering Conference—IECEC '92*, Society of Automotive Engineers, Warrendale, PA, 1992, pp. 1.95–1.100.

[3]Sridhar, K. R., "Mars Sample Return Mission with ISPP," *Journal of British Interplanetary Society*, Vol. 49, No. 11, 1996, pp. 435–440.

[4]Sridhar, K. R., "Mars Sample Return Mission with In-Situ Resource Utilization," *Journal of Propulsion and Power*, Vol. 11, No. 6, 1995, pp. 1356–1362.

[5]Wark, K., *Advanced Thermodynamics for Engineers*, McGraw–Hill, New York, 1995, pp. 378, 545.

[6]Vaniman, B. T., *Performance Characterization of Solid Oxide Electrochemical Cells*, M.S. Thesis, Dept. of Aerospace and Mechanical Engineering, Univ. of Arizona, Tucson, AZ, 1996.

[7]Ullman, H., *Keramische Gassensoren*, Akademie Verlag, Berlin, 1992, pp. 41, 81–84.

[8]Sridhar, K. R., and Vaniman, B. T., "Oxygen Production on Mars Using Solid Oxide Electrolysis," *Solid State Ionics*, Vol. 93, Nos. 3-4, 1997, pp. 321–328.

[9]Langmuir, I., "The Mechanism of the Catalytic Action of Platinum in the Reaction $2CO + O_2 = 2CO_2$ and $2H_2 + O_2 = 2H_2O$," *Transactions of the Faraday Society*, Vol. 17, Pt. 3, 1922, pp. 621–654.

[10]Etsell, T. H., and Flengas, S. N., "Overpotential Behavior of Stabilized Zirconia Solid Electrolyte Fuel Cells," *Journal of the Electrochemical Society*, Vol. 118, No. 12, 1971, pp. 1890–1900.

[11]Kittel, C., *Introduction to Solid State Physics*, 2nd ed., Wiley, New York, 1956, pp. 235–242.

[12]Trachtenberg, I., "Polarization Studies of Molten Carbonate Fuel Cell Electrodes," *Journal of the Electrochemical Society*, Vol. 111, No. 1, 1964, pp. 110–113.